Exp.-Nr. **A2-08/09**
Eingang: 15.05.2009
an PAC: 18.05.2009

Mainz Microtron MAMI

Collaboration A2: "Tagged Photons"
Spokesperson: A. Thomas

Proposal for an Experiment

"Transverse asymmetries T and F in η photoproduction in the $S_{11}(1535)$ region"

Spokespersons for the Experiment:

Sven Schumann, Institut für Kernphysik, University of Mainz, Germany
Bernd Krusche, Institut für Physik, University of Basel, Switzerland
Michael Ostrick, Institut für Kernphysik, University of Mainz, Germany

Abstract of Physics:

We propose to measure the target asymmetry T and the double-polarisation observable F for η photoproduction in order to investigate interference effects between the $S_{11}(1535)$ and the $D_{13}(1520)$ nucleon resonances and to determine the energy-dependent phase shift between s and d waves, which is not yet taken into account by isobar models (MAID, SAID) for η photoproduction.

Abstract of Equipment:

We require a beam of circularly polarised photons, energy-tagged by the Glasgow-Mainz tagging system, in combination with a transverse polarised 'Frozen Spin' butanol target. The reaction products will be detected using the Crystal Ball / TAPS 4π photon spectrometer; the PID detector and the cylindrical wirechambers will perform particle identification and track reconstruction for charged particles.

MAMI Specifications:

beam energy	1558 MeV
beam current	< 20 nA
beam polarisation	polarised

Photon Beam Specifications:

tagged energy range	632 – 1448 MeV
photon beam polarisation	circularly polarised

Equipment Specifications:

detectors	Crystal Ball, TAPS, MWPC, PID
target	Transverse polarised 'Frozen Spin' butanol target

Beam Time Request:

set–up/tests with beam	50 hours (parallel with proposal A2-09/09)
data taking	600 hours (parallel with proposal A2-09/09)

List of participating authors:

- **Institut für Physik, University of Basel, Switzerland**
  I. Jaegle, I. Keshelashvili, B. Krusche, Y. Maghrbi, F. Pheron, T. Rostomyan, D. Werthmüller
- **Institut für Experimentalphysik, University of Bochum, Germany**
  W. Meyer, G. Reicherz
- **Helmholtz–Institut für Strahlen- und Kernphysik, University of Bonn, Germany**
  R. Beck, A. Nikolaev
- **Massachusetts Institute of Technology , Cambridge, USA**
  A. Bernstein, W. Deconinck
- **JINR, Dubna, Russia**
  N. Borisov, A. Lazarev, A. Neganov, Yu.A. Usov
- **School of Physics, University of Edinburgh, UK**
  D. Branford, D.I. Glazier, T. Jude, M. Sikora, D.P. Watts
- **Petersburg Nuclear Physics Institute, Gatchina, Russia**
  V. Bekrenev, S. Kruglov, A. Koulbardis
- **Department of Physics and Astronomy, University of Glasgow, UK**
  J.R.M. Annand, D. Hamilton, D. Howdle, K. Livingston, J. Mancell, J.C. McGeorge, I.J.D. MacGregor, E.F. McNicoll, R.O. Owens, J. Robinson, G. Rosner
- **Department of Astronomy and Physics, Saint Mary's University Halifax, Canada**
  A.J. Sarty
- **Kent State University, Kent, USA**
  D.M. Manley
- **University of California, Los Angeles, USA**
  B.M.K. Nefkens, S. Prakhov, A. Starostin, I.M. Suarez
- **MAX-lab, University of Lund, Sweden**
  L. Isaksson
- **Institut für Kernphysik, University of Mainz, Germany**
  P. Aguar-Bartolome, H.J. Arends, S. Bender, A. Denig, E.J. Downie, N. Frömmgen, E. Heid, O. Jahn, H. Ortega, M. Ostrick, B.Oussena, P.B. Otte, S. Schumann, A. Thomas, M. Unverzagt
- **Institut für Physik, University of Mainz, D**
  J.Krimmer, W.Heil
- **University of Massachusetts, Amherst, USA**
  P.Martel, R.Miskimen
- **Institute for Nuclear Research, Moscow, Russia**
  G. Gurevic, R. Kondratiev, V. Lisin, A. Polonski
- **Lebedev Physical Institute, Moscow, Russia**
  S.N. Cherepnya, L.V. Fil kov, V.L. Kashevarov
- **INFN Sezione di Pavia, Pavia, Italy**
  A. Braghieri, A. Mushkarenkov, P. Pedroni
- **Department of Physics, University of Regina, Canada**
  G.M. Huber
- **Mount Allison University, Sackville, Canada**
  D. Hornidge

- **Tomsk Polytechnic University, Tomsk, Russia**
  A. Fix
- **Physikalisches Institut, University of Tübingen, Germany**
  P. Grabmayr, T. Hehl, D.G. Middleton
- **George Washington University, Washington, USA**
  W. Briscoe, T. Morrison, B.Oussena, B. Taddesse, M. Taragin
- **Catholic University, Washington, USA**
  D. Sober
- **Rudjer Boskovic Institute, Zagreb, Croatia**
  M. Korolija, D. Mekterovic, S. Micanovic, I. Supek

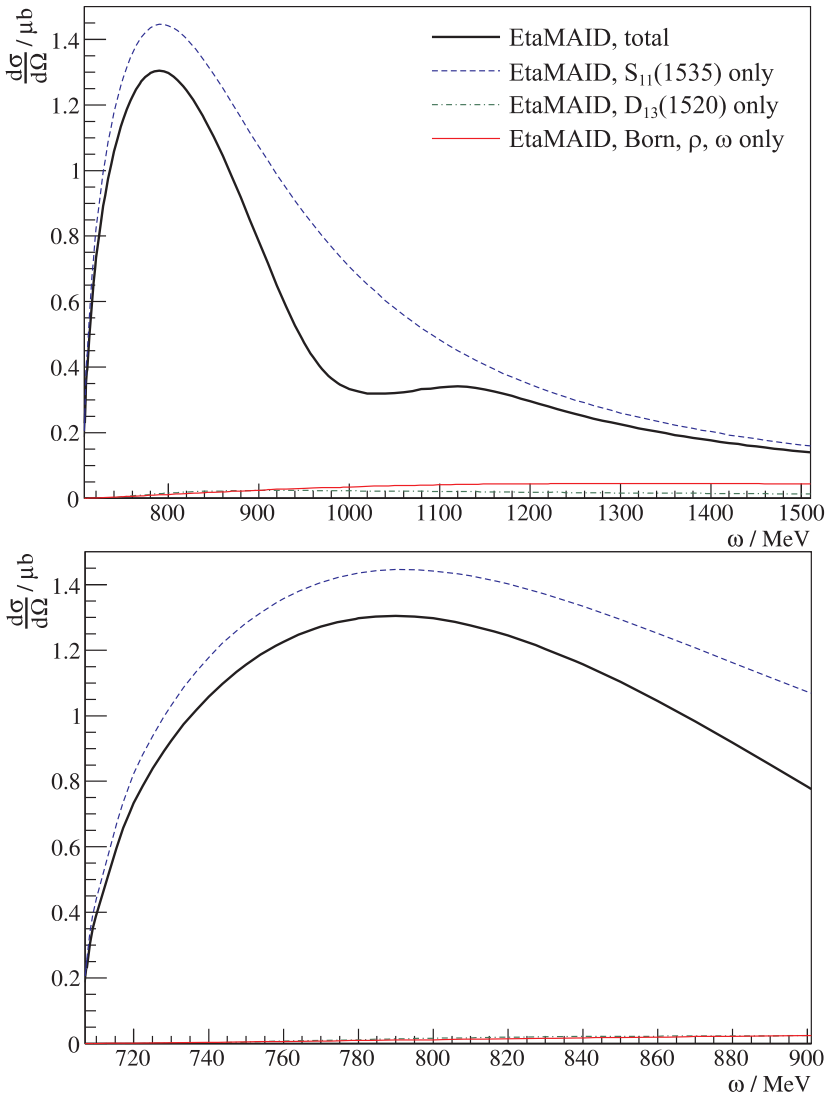

Figure 1: Contributions to the $\gamma p \to p\eta$ differential cross section at $\theta = 90°$ as predicted by EtaMAID [1].

1 Introduction

The photoproduction of η mesons offers the possibility to selectively probe certain resonances that are difficult to examine in reaction processes like pion scattering or pion photoproduction. The low-energy behaviour of η photoproduction ist vastly dominated by the excitation of the $S_{11}(1535)$ nucleon resonance, while contributions of other resonances in the same energy region, e.g. the $D_{13}(1520)$, are hard to discern. Figure 1 shows contributions of several processes ($S_{11}(1535)$ and $D_{13}(1520)$ resonances as well as non-resonant background processes) as predicted by the EtaMAID analysis [1]. However, as pointed out in [2], several polarisation observables offer access to these less-contributing resonances by exploiting interferences with the dominant E_{0+} multipole.

With the availability of experimental results for polarisation observables T and Σ from ELSA [3, 4] and GRAAL [5], in adition to the differential cross sections $\frac{d\sigma}{d\Omega}$ determined with TAPS in Mainz [6], it became possible to perform an almost model-independent analysis for $\ell = 0$ and $\ell = 2$ multipoles in the η threshold region [7], allowing a determination of $D_{13}(1520)$ contributions and resonance parameters.

Speaking in terms of a partial wave decomposition to electric and magnetic multipoles $E_{\ell\pm}$, $M_{\ell\pm}$

one can use the definition of helicity multipoles

$$\begin{aligned} A_{0+} &= E_{0+} \\ A_{2-} &= \frac{3}{2}M_{2-} - \frac{1}{2}E_{2-} \\ B_{1+} &= E_{1+} - M_{1+} \\ B_{2-} &= E_{2-} + M_{2-} \end{aligned}$$

which contribute to the observables $\frac{\mathrm{d}\sigma}{\mathrm{d}\Omega}$, Σ and T according to

$$\begin{aligned} \frac{\mathrm{d}\sigma}{\mathrm{d}\Omega} \equiv \sigma_0 &= \frac{q}{k}\left(|E_{0+}|^2 - 2(3\cos^2\theta - 1)\cdot \mathrm{Re}\{E_{0+}^* A_{2-}\}\right) \\ \sigma_0\Sigma &= 3\frac{q}{k}\sin^2\theta \cdot \mathrm{Re}\{E_{0+}^* B_{2-}\} \\ \sigma_0 T &= 3\frac{q}{k}\sin\theta\left(\mathrm{Im}\{E_{0+}^* B_{1+}\} - \cos\theta\cdot\mathrm{Im}\{E_{0+}^* B_{2-}\}\right) \end{aligned}$$

where q and k describe the η and photon momenta, respectively. As the cross section σ_0 mainly depends on $|E_{0+}|^2$, it shows a very strong S_{11} dominance, with little sensitivity to other multipole contributions. The polarisation observables Σ and T show sensitivity to both the real and the imaginary part of the interference term $E_{0+}^* B_{2-}$, describing the interference between s- and d-wave, giving access also to properties of the $D_{13}(1520)$ state.
Particularly the imaginary part $\mathrm{Im}\{E_{0+}^* B_{2-}\}$ of this interference term, available through T, is an interesting parameter, as virtually all isobar models predict this value to be close to zero. This is due to the fact that in Breit-Wigner parametrisation both the $S_{11}(1535)$ and $D_{13}(1520)$ resonances are close in energy and have similar widths. With these assumptions the relative s-d wave phase $\delta_0 - \delta_2$ should be at small negative values (as the S_{11} state is a little bit higher in energy) and also should be rather constant. So, as the relative phase between the E_{0+} and B_{2-} multipoles is given by

$$\tan(\delta_{E_{0+}} - \delta_{B_{2-}}) = \frac{\mathrm{Im}\{E_{0+}^* B_{2-}\}}{\mathrm{Re}\{E_{0+}^* B_{2-}\}}$$

isobar models like EtaMAID or SAID [8] assume a vanishing imaginary part of $E_{0+}^* B_{2-}$.
Interestingly, a comparision with the only existing experimental dataset for the $\gamma p \to p\eta$ target asymmetry T from Bock et al. [3] indicates, that this assumption is not fulfilled especially in the lower energy region (see figure 2). In particular, the theoretical models do not reproduce the additional $\sin(2\theta)$ modulation with its zero-crossing node at $\theta \approx 90°$, which is quite distinctive in the experimental results especially around $\omega = 737\,\mathrm{MeV}$.
However, a model-independent fit to the existing data for T using the relation

$$\sigma_0 T = 3\frac{q}{k}\sin\theta\left(\mathrm{Im}\{E_{0+}^* B_{1+}\} - \cos\theta\cdot\mathrm{Im}\{E_{0+}^* B_{2-}\}\right)$$

yields non-vanishing results for the imaginary part of $E_{0+}^* B_{2-}$, leading to a large enhancment of the d wave magnitude of B_{2-} and, more important, in an energy-dependent phase shift $\delta_{E_{0+}} - \delta_{B_{2-}}$, the so-called 'phase rotation' (see figure 3), which raises up to around 90° in the threshold region.
This unexpected relative phase shift between the S_{11} and D_{13} states can be taken as an indication that at least one of these contributing resonances, supposedly the $S_{11}(1535)$, behaves quite different from other known nucleon resonances and might be not a nucleon resonance in a conventional sense but a completely different phenomenon, as, for example, suggested by [9].
For a precise investigation of these s-d wave interference effects in the η threshold region we propose to perform a measurement of the target asymmetry T to confirm the modulation in θ and the node structure. In comparison to the exisiting Bonn measurement [3] we are aiming for higher resolution and accuracy with respect to both the beam energy ω and the polar angle θ.

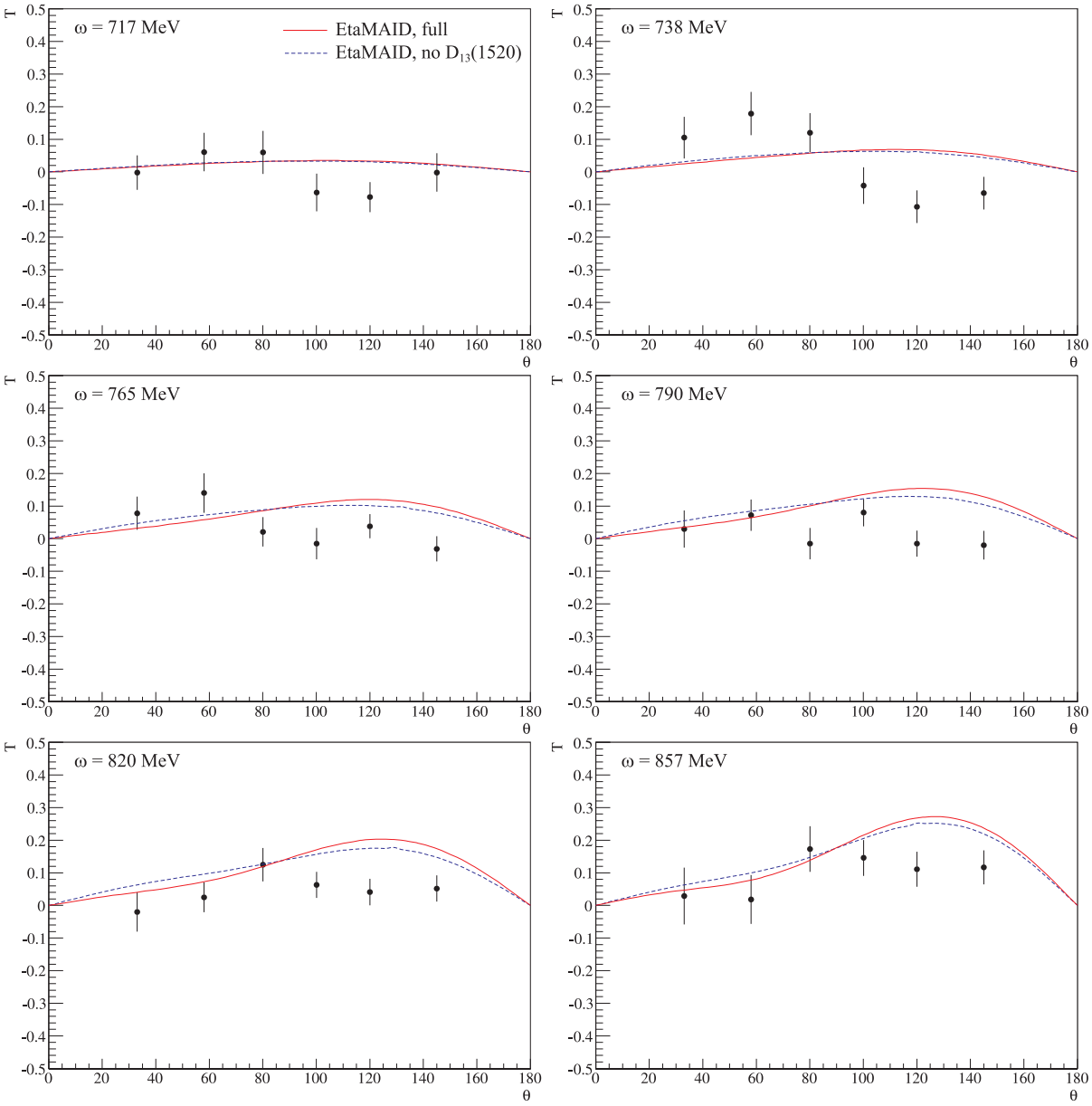

Figure 2: Target asymmetries T for $\gamma p \to p\eta$ at different photon energies ω. The solid red and dashed blue lines show EtaMAID calculations with and without $D_{13}(1520)$ contributions; experimental data are from Bock et al. [3].

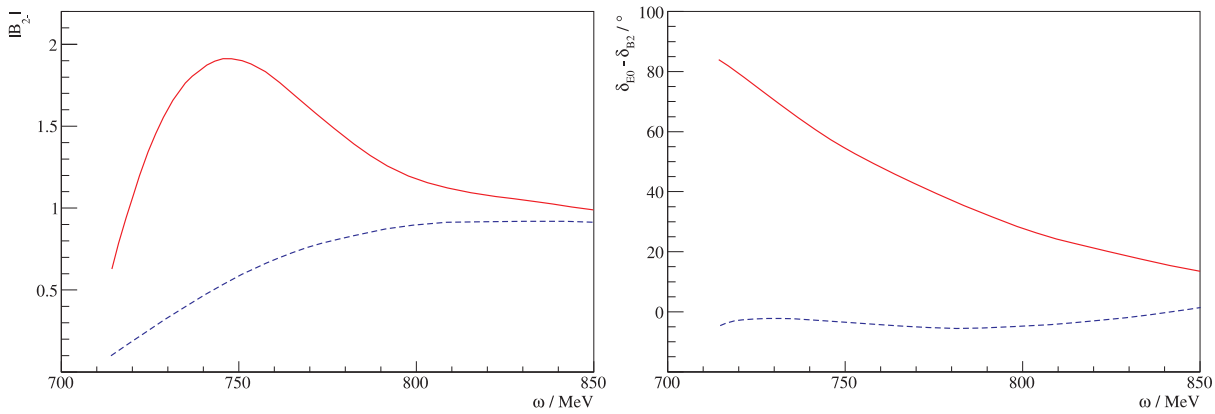

Figure 3: Magnitude $|B_{2-}|$ (left panel) and s-d wave phase shift $\delta_{E_{0+}} - \delta_{B_{2-}}$ (right panel) for the standard EtaMAID calculation (blue dashed line) and for an ad-hoc consideration of $\mathrm{Im}\{E^*_{0+}B_{1+}\}$ (solid red line) obtained from a fit to the experimental results for T.

This will allow to precisely determine size and energy dependence of the s-d wave phase rotation and clarify the interference of S_{11} and D_{13} states in the low-energy region.
In general, the cross section for single meson production with polarised beam (linear or circular) and polarised target (transverse or longitudinal) is given by

$$\begin{aligned}\left.\frac{\mathrm{d}\sigma}{\mathrm{d}\Omega}\right|_{\mathrm{pol}} = \frac{\mathrm{d}\sigma}{\mathrm{d}\Omega}\cdot\big[1 \;&-\; p^{\gamma}_{\mathrm{lin}}\Sigma\cos(2\varphi)\\ &-\; p^{\mathrm{T}}_x p^{\gamma}_{\mathrm{lin}} H\sin(2\varphi) \;+\; p^{\mathrm{T}}_x p^{\gamma}_{\mathrm{circ}} F\\ &+\; p^{\mathrm{T}}_y T \;-\; p^{\mathrm{T}}_x p^{\gamma}_{\mathrm{lin}} P\cos(2\varphi)\\ &+\; p^{\mathrm{T}}_z p^{\gamma}_{\mathrm{lin}} G\sin(2\varphi) \;-\; p^{\mathrm{T}}_z p^{\gamma}_{\mathrm{circ}} E\big]\end{aligned}$$

where $p^{\gamma}_{\mathrm{lin,circ}}$ and $p^{T}_{x,y,z}$ denote the degrees of polarisation for the incoming photon beam and the target nucleons, respectively. This cross section simplifies to

$$\left.\frac{\mathrm{d}\sigma}{\mathrm{d}\Omega}\right|_{\mathrm{pol}} = \frac{\mathrm{d}\sigma}{\mathrm{d}\Omega}\cdot\big[1 \;+\; p^{\mathrm{T}}_x p^{\gamma}_{\mathrm{circ}} F \;+\; p^{\mathrm{T}}_y T\big]$$

in case of a transverse polarised target and a circular polarised photon beam, allowing a determination of the target asymmetry T and the double-polarisation observable F.
As shown in figure 4, the isobar model calculations like EtaMAID or SAID in their standard configurations are not able to reproduce the node structure in T, as indicated by the existing dataset [3] at lower photon energies. In addition, a modified EtaMAID calculation with an ad-hoc consideration of the phase rotation is shown to demonstrate the sensitivity to this effect, which is high close to threshold, still sizable around the S_{11} Breit-Wigner mass around $\omega = 790$ MeV ($W = 1537$ MeV) but nearly vanished at $\omega > 850$ MeV ($W > 1573$ MeV). It should be noted, however, that with rising beam energy the different model calculations show quite significant discrepancies in the angular dependence of T.
As the target asymmetry T is one of the three single polarisation observables in single meson production, it is already accessible with only a polarised target and an unpolarised photon beam. However, using a circularly polarised photon beam does not affect this asymmetry but gives also access to the double-polarisation observable F without any further experimental effort. There are also no difficulties in disentagling these observables, as the target asymmetry T can be extracted

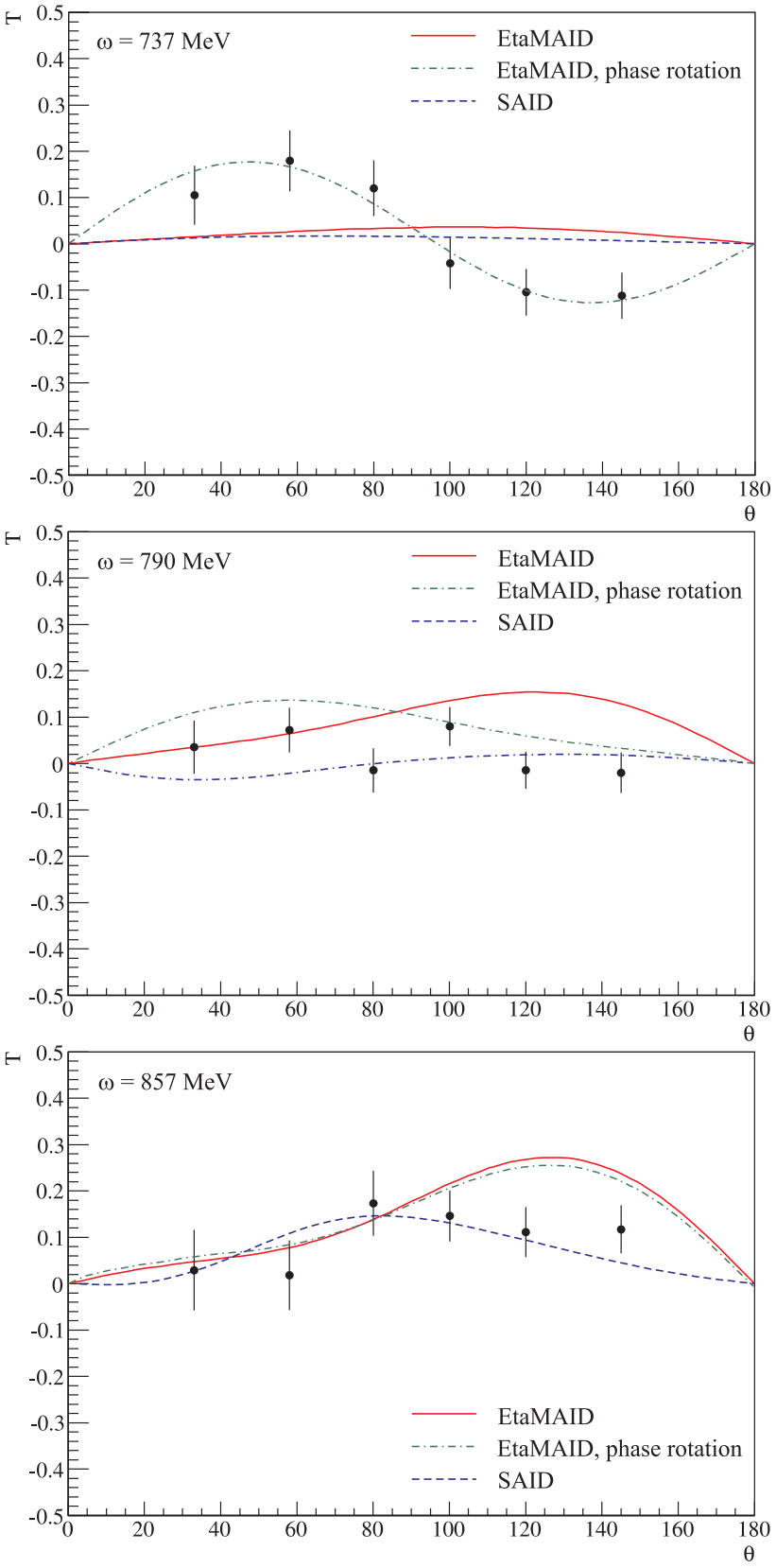

Figure 4: Model calculations for the target asymmetry T at different beam energies ω. The green dash-dotted and red solid lines show EtaMAID predictions with and without an ad-hoc consideration of the phase rotation, the blue dashed line represents the SAID standard solution. Data points are from Bock et al. [3].

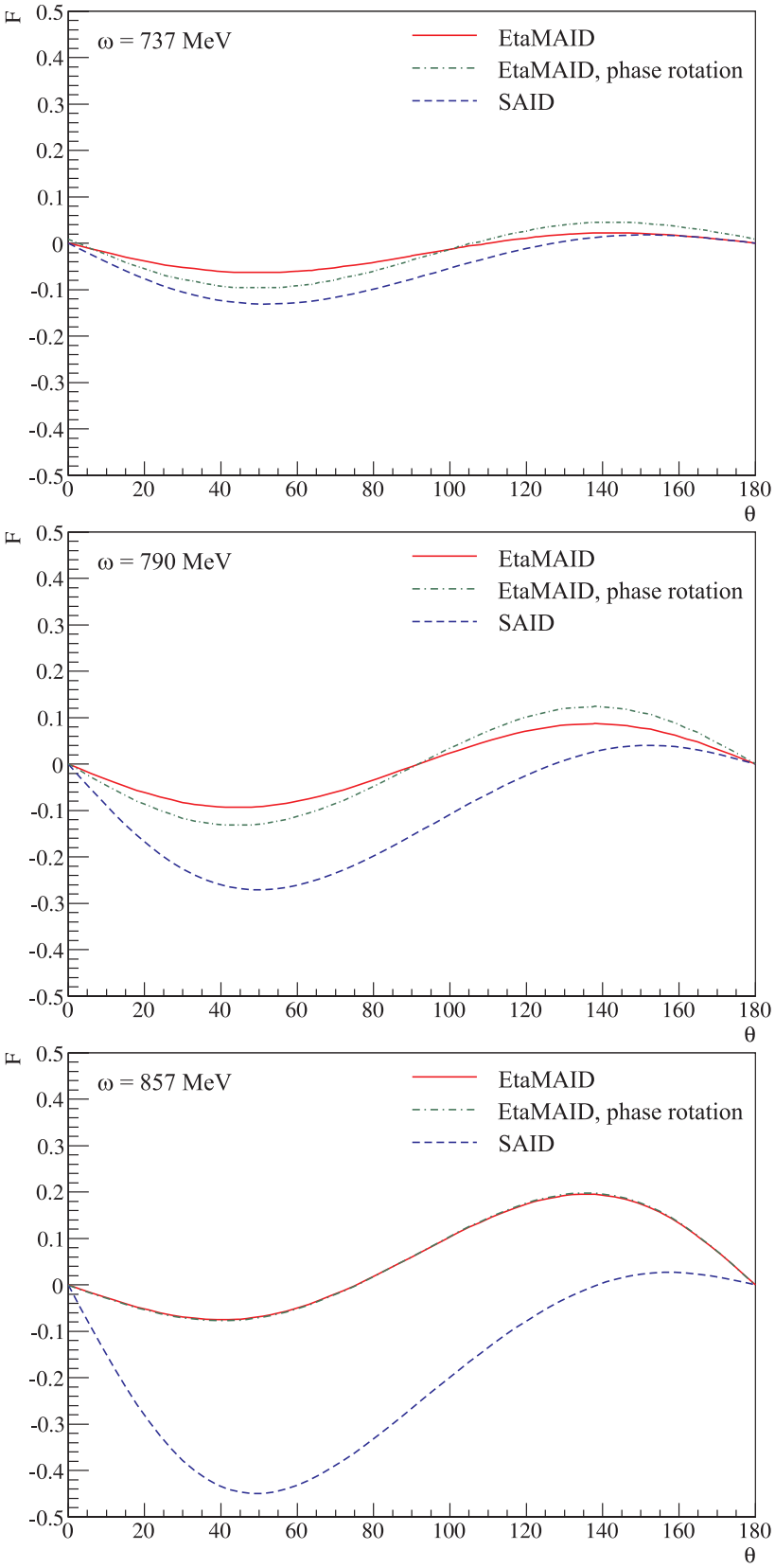

Figure 5: Model calculations for the double-polarisation observable F at different beam energies ω. The green dash-dotted and red solid lines show EtaMAID predictions with and without an ad-hoc consideration of the phase rotation, the blue dashed line represents the SAID standard solution.

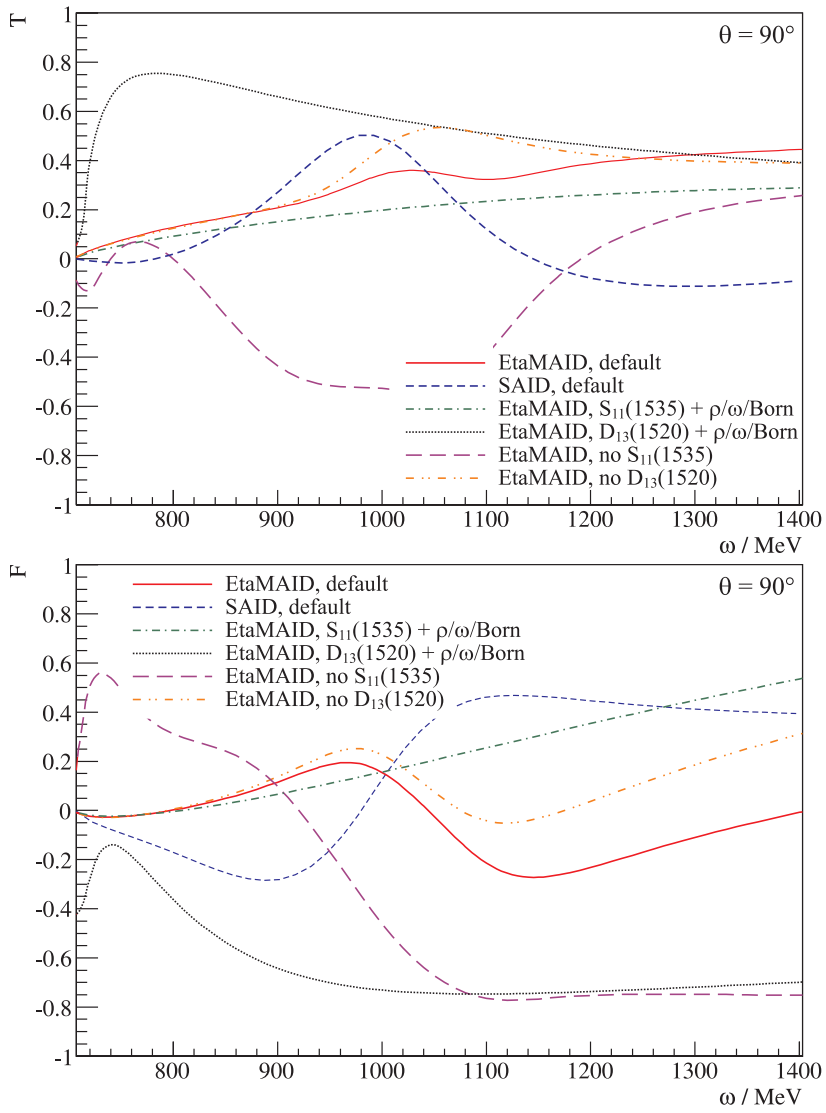

Figure 6: Beam energy dependence of T and F at a fixed polar angle $\theta = 90°$, as predicted by EtaMAID and SAID calculations. In case of EtaMAID the full solution as well as results either with only or without the $S_{11}(1535)$ and $D_{13}(1520)$ resonances are shown.

integrating over both helicity states $\lambda = \pm 1$ of the incoming circularly polarised photons, which eliminates any contributions from F. In contrast, the double-polarisation observable F can be evaluated from the asymmetry for different beam helicity states λ for a fixed alignment in the azimuthal angle ϕ of the transverse target polarisation.

Figure 5 shows the angular dependence of F for different beam energies ω in the energy region of the $S_{11}(1535)$ resonance as predicted by isobar model calculations; in case of EtaMAID predictions are again with and without the inclusion of an s-d phase shift. The phase rotation also affects this observable, although to a lesser extent than in case of the target asymmetry T. Interestingly, there are even bigger discrepancies between different model predictions than in case of T, especially away from threshold in the energy region $\omega > 850\,\text{MeV}$. As there is no experimental data for this observable yet, measuring F for the first time will put further constraints to isobar models and partial wave analyses for η production, helping to solve these discrepancies.

Finally, figure 6 shows the energy dependence of both T and F for a fixed polar angle $\theta = 90°$ and beam energies from threshold ($\omega = 707$ MeV) up to the maximum photon beam energy $\omega \approx 1400$ MeV available at MAMI-C. This demonstrates the big discrepancies between SAID

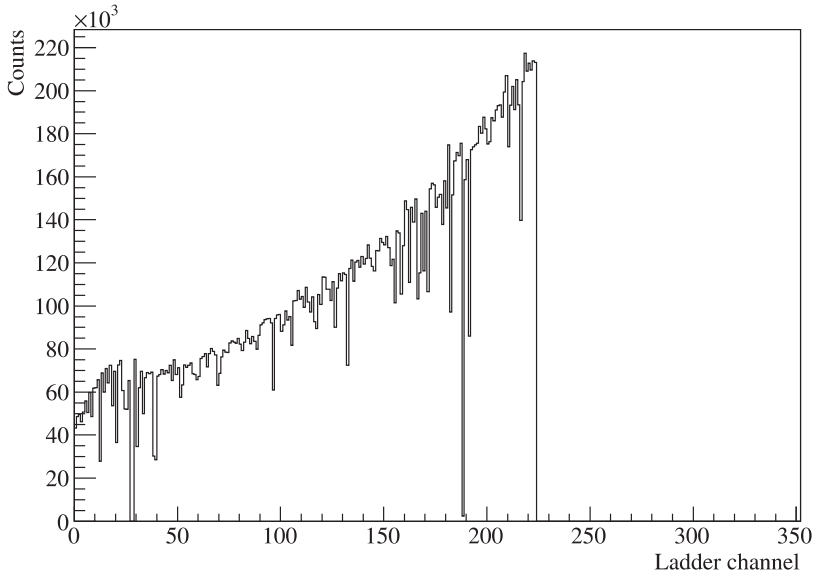

Figure 7: Bremsstrahlung spectrum obtained with the Glasgow tagger. Detector channels 225 to 352 were disabled here to increase the photon flux in the remaining high-energy part of the spectrum.

and EtaMAID calculations, especially at higher photon energies $\omega \gtrsim 1000\,\mathrm{MeV}$, as well as (in case of EtaMAID) the sensitivity of T and F to different resonance contributions, namely the $S_{11}(1535)$ and $D_{13}(1520)$.

2 Experimental issues

We propose to use the Crystal Ball as central detector in conjunction with TAPS as forward wall for measurements of η photoproduction using a transverse polarised butanol target and a tagged photon beam with energies up to $\omega = 1448\,\mathrm{MeV}$ ($W = 1897\,\mathrm{MeV}$). General details of the experimental setup, such as the photon tagging system, the polarised target system and the Crystal Ball / TAPS detector systems are described in appendix A.

The tagging system in conjunction with a polarised electron beam ($E_0 = 1558\,\mathrm{MeV}$, $P_e \simeq 85\%$) from MAMI-C will provide a circularly polarised photon beam with polarisation degrees varying between $P_\gamma^{\mathrm{circ}} = 0.48$ (η threshold at $\omega = 707\,\mathrm{MeV}$) and $P_\gamma^{\mathrm{circ}} = 0.81$ (maximum energy $\omega = 1448\,\mathrm{MeV}$), giving an average photon polarisation of $\bar{P}_\gamma^{\mathrm{circ}} = 0.6$. Due to the typical $\frac{1}{\omega}$ distribution of the resulting bremsstrahlung spectrum the maximum count rate is achieved by the lowest-energy (in terms of photon energy ω) tagger channels; in order to either increase the available photon flux at higher energies or reduce the data acquisition load, detector channels in the lower-end part will be switched off. With tagger channels 1 to 224 activated, this will result in a tagged photon energy range from 632 to 1448 MeV (see figure 7).

Measuring the target asymmetry T and the double-polarisation observable F requires transverse polarised target nucleons, which will be available through the new Mainz 'Frozen Spin' butanol (C_4H_9OH) target that is expected to be operational within 2009. During measurements the target polarisation will be retained by a superconducting coil ($B \simeq 0.4\,\mathrm{T}$) with an appropriate field configuration for transverse alignment of proton spins. General parameters of the polarised target can be found in appendix A.2.

Detection and reconstruction of η mesons will be done with the Crystal Ball / TAPS detector setup and the inner detector systems for particle identification and track reconstruction (see appendices A.3 and A.4). Because of its high-granularity and large acceptance the CB/TAPS setup is a suitable detector system for measurements of reactions with multi-photon final states

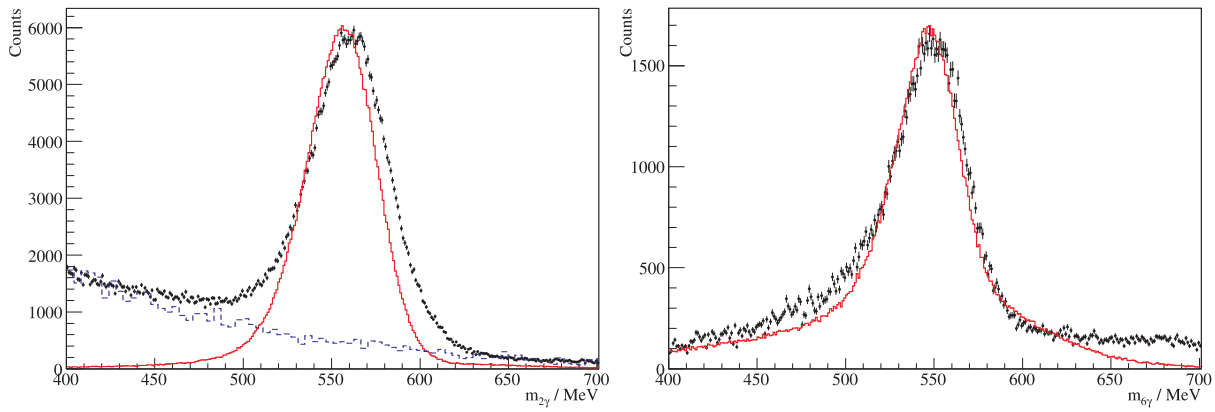

Figure 8: Invariant mass spectra for events with 2 (left panel) and 6 (right panel) photons for both a simulation of $\gamma p \to p\eta$ (solid red line) and data (black points). Additionally, for the 2 photon case a simulation of $\gamma p \to p\pi^0\pi^0$ is shown (dashed blue line).

like in $\pi^0 \to 2\gamma$, $\eta \to 2\gamma$ or $\eta \to 3\pi^0 \to 6\gamma$. The typical width of reconstructed invariant π^0 masses is about $\sigma = 9\,\mathrm{MeV}$. For η mesons, invariant mass distributions for both neutral decay modes $\eta \to 2\gamma$ (BR = 39.38%) and $\eta \to 3\pi^0 \to 6\gamma$ (BR = 32.51%) are shown in fig. 8, giving widths of about $\sigma = 21\,\mathrm{MeV}$. At least for the 6γ case this value can, however, be improved when using the additional mass constraints to the intermediate $3\pi^0$.
Comparisons of experimental data from 2007 and simulations of $\gamma p \to p\eta$ and $\gamma p \to p\pi^0\pi^0$ (solid red and dashed blue line in fig. 8), show that the selection of 6 neutral cluster events already gives quite a clean identification of $\eta \to 3\pi^0 \to 6\gamma$ decays, while in the 2-photon case there is a significant amount of (combinatorical) background mainly from double π^0 production where 2 out of the 4 decay photons were not detected. Reduction of such background and further identification of the reaction process $\gamma p \to p\eta$, however, is possible using cuts on reaction kinematics like missing mass or missing energy (see fig. 9 for resulting missing mass distributions from 2007 data and simulated $\gamma p \to p\eta$ reactions). Simulations based on EtaMAID predictions give a total detection and reconstruction efficiency of about $\varepsilon_{CB} = 30\%$ when analysing both neutral decay modes $\eta \to 2\gamma$ and $\eta \to 3\pi^0 \to 6\gamma$.

3 Event rates and beamtime estimate

The target asymmetry T in the reaction $\gamma p \to \eta p$ is determined from the measured count-rate asymmetry T_{meas} by

$$T = \frac{\eta'_d}{P_p^y} T_{\mathrm{meas}} = \frac{\eta'_d}{P_p^y} \frac{N_\phi - N_{\phi+\pi}}{N_\phi + N_{\phi+\pi}}$$

where P_p^y is the degree of target polarisation in y-direction (with respect to the reaction plane) and η'_d is the effective target dilution factor from the butanol target material. N_ϕ and $N_{\phi+\pi}$ are the total event numbers for two directions ϕ and $\phi + \pi$ of target polarisation with a difference of 180°.
For the double-polarisation observable F a similar relation is given by

$$F = \frac{\eta'_d}{P_p^x \cdot P_\gamma^{\mathrm{circ}}} F_{\mathrm{meas}} = \frac{\eta'_d}{P_p^x \cdot P_\gamma^{\mathrm{circ}}} \frac{N_{\lambda=+1} - N_{\lambda=-1}}{N_{\lambda=+1} + N_{\lambda=-1}}$$

where the target polarisation in x-direction (with respect to the reaction plane) is used and additionally the circular beam polarisation P_γ^{circ} enters. In this case the event numbers $N_{\lambda=\pm1}$ for two helicity states $\lambda = \pm 1$ of the incoming photons and a fixed target polarisation direction ϕ are used to calculate the measured asymmetry F_{meas}.

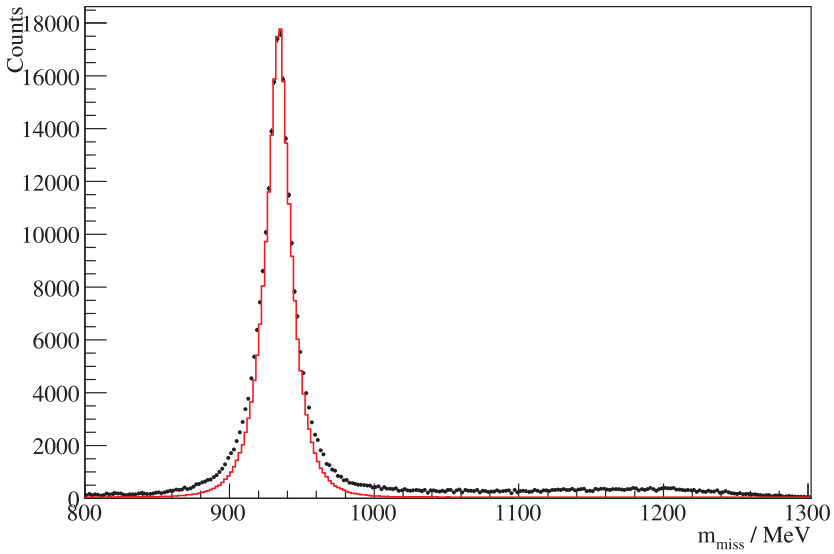

Figure 9: Missing mass calculated from the initial γp state and the reconstructed η meson for both a $\gamma p \to p\eta$ simulation (solid red line) and 2007 data (black points).

The total dilution factor η_d can be estimated using the number of free protons in the used butanol (C_4H_9OH) target material which is given by $\eta_d = \frac{74}{10}$. This is, however, not a realistic assumption for the effective dilution factor η'_d, as the cross section for (quasi-free) η production on nuclei with mass number A scales like $\sigma_A \sim A^{2/3}$ [10]. Furthermore, comparing the cross sections σ_n and σ_p for η production on neutrons and protons, a ratio $\frac{\sigma_n}{\sigma_p} = 0.66$ is reported for photon energies up to $\omega = 850\,\text{MeV}$ [11]. With these relations the dilution factor by target nuclei other than hydrogen is already reduced to $\eta_d \approx 3.37$. Also, a significant amount of background from unpolarised ^{12}C, ^{16}O and ^{4}He nuclei can already be removed using kinematical cuts (missing mass, missing energy, see figure 10). Simulations including reactions on free protons as well as quasi-free processes on bound nucleons suggest an effective dilution factor $\eta'_d = 1.55$.
With a maximum photon flux of $\dot{N}_\gamma \simeq 5 \cdot 10^7\,\text{s}^{-1}$ over the complete tagged energy range the polarised target can sustain, and based on previous experiences with the CB/TAPS detector setup at MAMI-C as well as simulations of $\gamma p \to \eta p$, the following parameters are used for count-rate estimations and beam-time request:

- Incoming electron beam energy: $E_0 = 1558\,\text{MeV}$
- Tagged photon energy range: 632 to 1448 MeV (Tagger channels 1 to 224)
- Total electron count rate over tagged energy region: $\dot{N}_e = 2.04 \cdot 10^7\,\text{s}^{-1}$
- Tagging efficiency: $\varepsilon_{\text{tag}} = 0.7$
- Total photon flux over tagged energy region: $\dot{N}_\gamma = 1.43 \cdot 10^7\,\text{s}^{-1}$
- Number of polarised protons in a 2 cm 'Frozen Spin' butanol target: $N_p = 0.91 \cdot 10^{23}\,\text{cm}^{-2}$
- Total cross section for $\gamma p \to p\eta$: $\sigma_{tot} = 16\,\mu\text{b}$ (at $\omega = 780\,\text{MeV}$)
- Average transverse target polarisation: $P_p^{\text{trans}} = 0.7$
- Average circular beam polarisation: $P_\gamma^{\text{circ}} = 0.6$
- Detection and reconstruction efficiency for $\gamma p \to p\eta$ (analysing both neutral η decay modes $\eta \to 2\gamma$ and $\eta \to 3\pi^0 \to 6\gamma$): $\varepsilon_{CB} = 0.3$

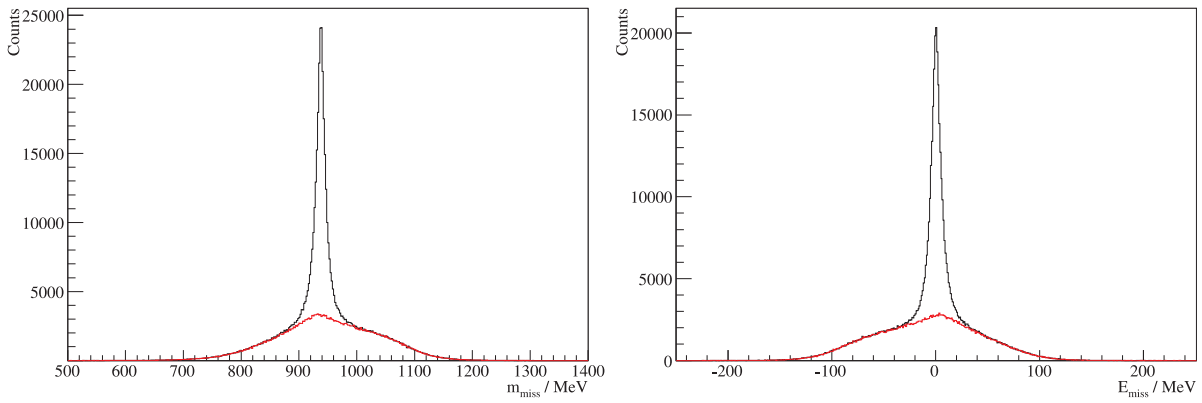

Figure 10: Missing mass (left panel) and missing energy (right panel) distributions from $\gamma p \to p\eta$ simulations with butanol target. The black line contains contributions from all target atoms, including ^{1}H, while the red line only covers background from quasi-free processes on unpolarised ^{12}C and ^{16}O nuclei.

- Effective dilution factor: $\eta'_d = 1.55$
- Trigger conditions: CB energy sum $\Sigma_{CB} > 350$ MeV and cluster multiplicity $M \geq 3$ in combination with (downscaled) $M \geq 2$.
- Data acquistion capability: 800 events/s at a DAQ livetime of 70%

These parameters will result in a rate of around 3900 *reconstructed* reactions $\gamma p \to p\eta$ per hour. For the target asymmetry T and investigation of the *s*-*d* phase shift in the $S_{11}(1535)$ region (up to $\omega \simeq 950$ MeV) we aim for a statistical accuracy of $\Delta T \simeq 0.03$ at $\theta = 90°$ with bin sizes of $\Delta\omega = 10$ MeV in photon energy and $\Delta\theta = 12°$ in the angular distribution. Simulations show that this would require around $2 \cdot 10^6$ reconstructed $\gamma p \to p\eta$ events (see figure 11 and upper panel of figure 13), corresponding to 510 hours of data taking. As about 15% of the total beam time will be used for target repolarisation (∼6 hours every 2 days) and tagging efficiency measurements, we request a total beam time of **600 hours**. At higher beam energies, this would still result in statistical accuracies varying between $\Delta T \simeq 0.06$ at $\omega = 1,1$ GeV and $\Delta T \simeq 0.10$ at $\omega = 1,4$ GeV.
With respect to the double-polarisation observable F these 600 hours of total beam time will give a statistical precision of $\Delta F \simeq 0.04$ at $\theta = 90°$ in the $S_{11}(1535)$ region with bin sizes of $\Delta\omega = 20$ MeV in photon energy and $\Delta\theta = 12°$ in the polar angle distribution. Above 1 GeV beam energy accuracies between $\Delta F \simeq 0.06$ at $\omega = 1,1$ GeV and $\Delta F \simeq 0.09$ at $\omega = 1,4$ GeV can be achieved (see figure 12 and lower panel of figure 13).

References

[1] W.T. Chiang et al.: *An isobar model for η photo- and electroproduction on the nucleon*, Nucl. Phys. **A 700** (2002) 429

[2] L. Tiator et al.: *The ηNN coupling in eta photoproduction*, Nucl. Phys. **A 580** (1994) 455

[3] A. Bock et al.: *Measurement of the Target Asymmetry of η and π^0 Photoproduction on the Proton*, Phys. Rev. Lett. **81** (1998) 534

[4] D. Elsner et al.: *Measurement of the beam asymmetry in η photoproduction off the proton*, Eur. Phys. J. **A 33** (2007) 147

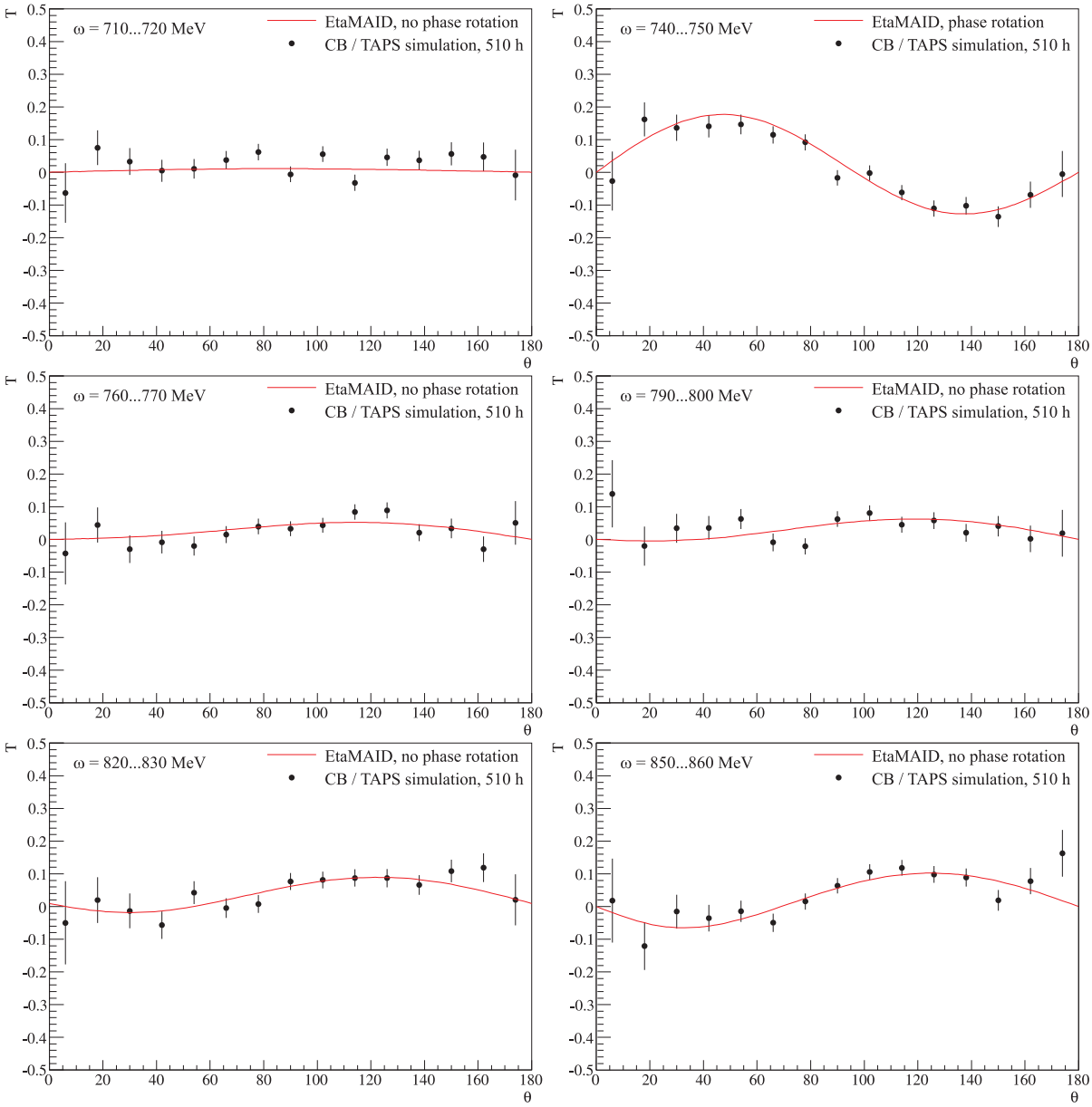

Figure 11: Simulation of target asymmetries T for $\gamma p \to p\eta$ with CB / TAPS at different photon energies ω in the $S_{11}(1535)$ region. The number of simulated events corresponds to 510 hours of data taking. The solid red line shows the EtaMAID calculation used for the polarisation-dependent angular distribution of simulated η mesons. The phase rotation effect is only included in the $\omega = 740$ MeV calculation (upper right panel).

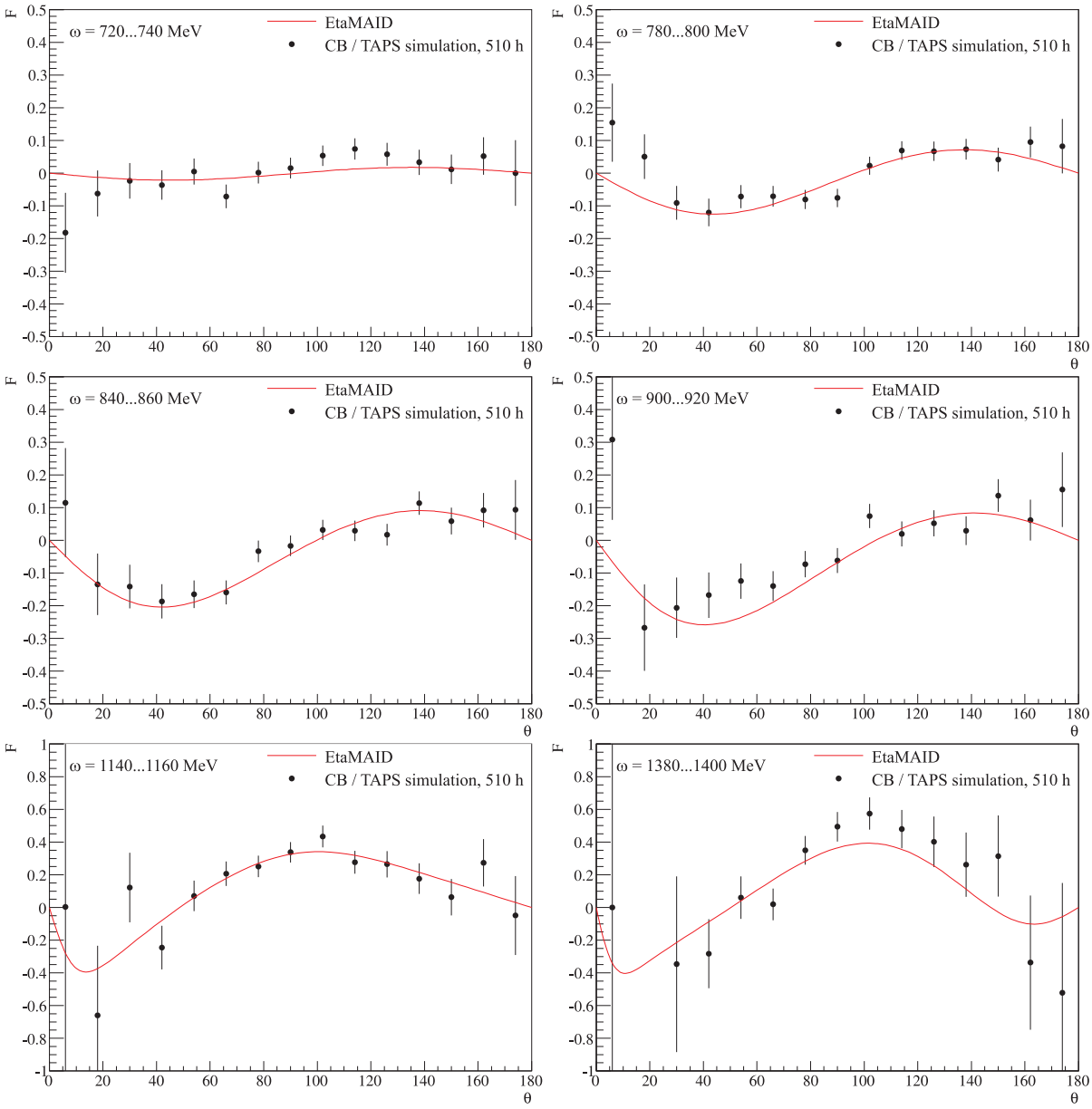

Figure 12: Simulation of double-polarisation observable F results for $\gamma p \to p\eta$ with CB / TAPS at different photon energies ω. The number of simulated events corresponds to 510 hours of data taking. The solid red line shows the EtaMAID calculation used for the polarisation-dependent angular distribution of simulated η mesons.

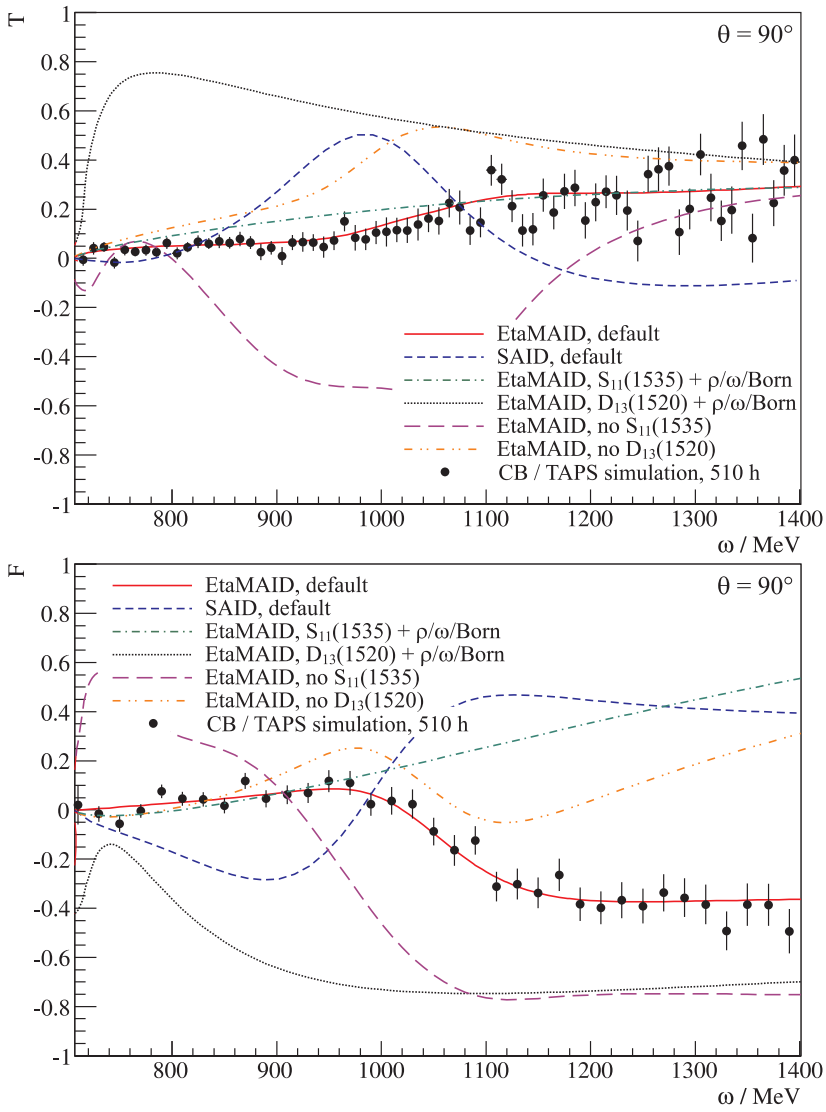

Figure 13: Simulation of T and F results with CB / TAPS at a fixed polar angle $\theta = 90°$ and different beam energies ω. The number of simulated events corresponds to 510 hours of data taking. The solid red line shows the EtaMAID calculation used for the polarisation-dependent distribution of simulated η mesons. Results of SAID and EtaMAID with selected contributions are shown to demonstrate the expected sensitivity.

[5] J. Ajaka et al.: *New Measurement of Σ Beam Asymmetry for η Meson Photoproduction on the Proton*, Phys. Rev. Lett. **81**, (1998) 1797

[6] B. Krusche et al.: *Near Threshold Photoproduction of η Mesons off the Proton* Phys. Rev. Lett. **74** (1995) 3736

[7] L. Tiator et al.: *Analysis of resonance multipoles from polarization observables in η photoproduction*, Phys. Rev. **C 60** (1999) 035210

[8] CNS Data Analysis Center, `http://gwdac.phys.gwu.edu/`

[9] N. Kaiser et al.: *Chiral dynamics and the $S_{11}(1535)$ nucleon resonance*, Phys. Lett. **B 362** (1995) 23

[10] M. Röbig-Landau et al.: *Near Threshold photoproduction of η-mesons from complex nuclei*, Phys. Lett. **B 373** (1996) 45

[11] B. Krusche et al.: *Near-threshold photoproduction of η-mesons from the deuteron*, Phys. Lett. **B 358** (1995) 40

A Experimental apparatus

A.1 Photon Beam

The A2 photon beam is derived from the production of Bremsstrahlung photons during the passage of the MAMI electron beam through a thin radiator. The resulting photons can be circularly polarised, with the application of a polarised electron beam, or linearly polarised, in the case of a crystalline radiator. The degree of polarisation achieved is dependent on the energy of the incident photon beam (E_0) and the energy range of interest, but currently peaks at ∼75% for linear polarisation (Fig. 14) and ∼85% for circular polarisation (Fig. 15). The maximum degree of linear polarisation should be further improved by 5 to 10% by the end of 2009 when the collimation and beam monitoring systems will be optimised for MAMI-C during the installation of the Frozen Spin Target. The Glasgow Photon Tagger (Fig 16) provides energy tagging of the photons by detecting the post-radiating electrons and can determine the photon energy with a resolution of 2 to 4 MeV depending on the incident beam energy, with a single-counter time resolution $\sigma_t = 0.117$ ns [2]. Each counter can operate reliably to a rate of ∼1 MHz, giving a photon flux of $2.5 \cdot 10^5$ photons per MeV. Photons can be tagged in the momentum range from 4.7 to 93.0% of E_0.
To augment the standard focal plane detector system and make use of the Tagger's intrinsic energy resolution of 0.4 MeV (FWHM), there exists a scintillating fibre detector ('Tagger Microscope') that can improve the energy resolution by a factor of about 6 for a ∼100 MeV wide region of the focal plane (dependent on its position) [4].

A.2 Frozen-Spin Target

Polarisation experiments using high density solid-state targets in combination with tagged photon beams can reach the highest luminosities. For the double polarisation measurements planned with the Crystal Ball detector on polarised protons and deuterons a specially designed, large horizontal ^{3}He/^{4}He dilution refrigerator was built in cooperation with the Joint Institute for Nuclear Research (JINR) Dubna (see Figure 17). It has minimum limitations for the particle detection and fits into the central core of the inner Particle Identification Detector (PID2). This was achieved by using the frozen spin technique with the new concept of placing a thin superconducting holding coil inside the polarisation refrigerator. Longitudinal and transverse polarisations will be possible.

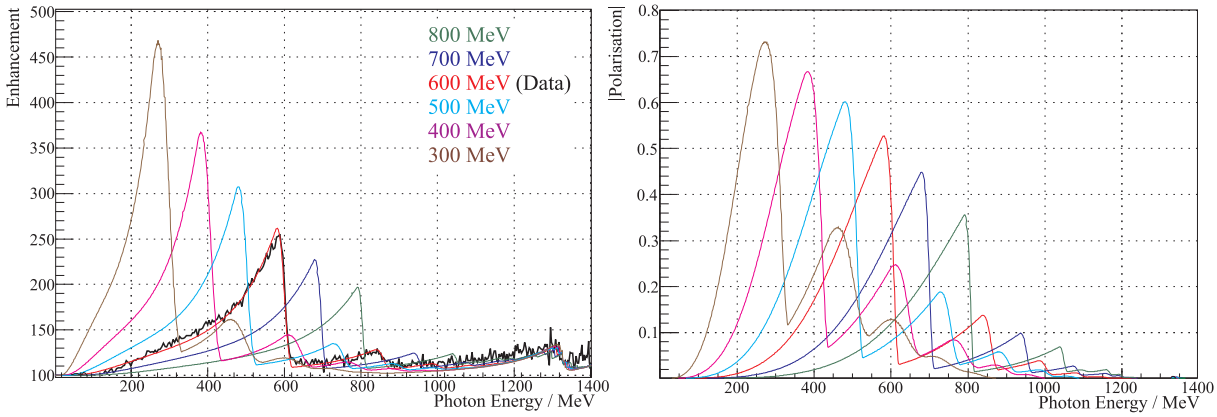

Figure 14: Linear polarisation available with the current collimation system for a variety of crystal orientations. The thin black lines are data obtained during recent MAMI-C runs.

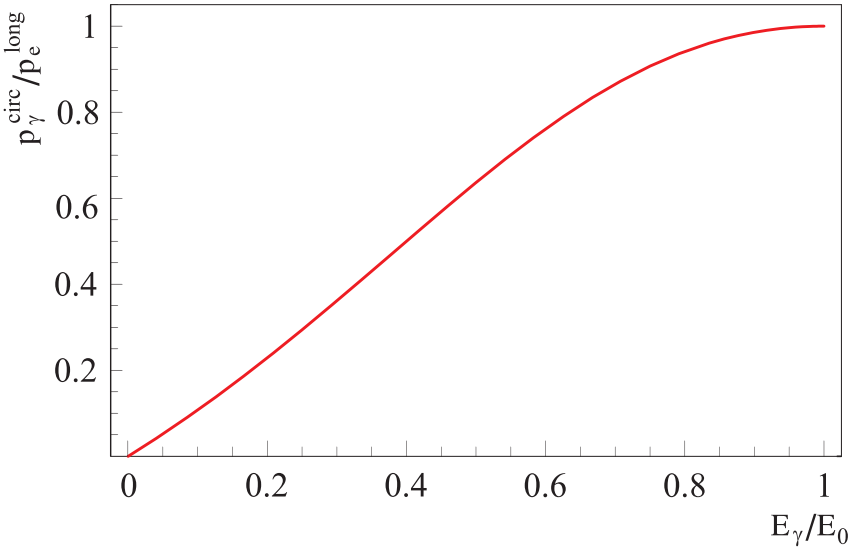

Figure 15: Helicity transfer from the electron to the photon beam as function of the energy transfer. The MAMI beam polarisation is $P_e \approx 85\%$.

Highest nucleon polarisation in solid-state target materials is obtained by a microwave pumping process, known as 'Dynamic Nucleon Polarisation' (DNP). This process is applicable to any nucleus with spin and has already been used in different experiments with polarised proton and deuteron targets. The geometric configuration of the target is the same for the polarised proton and neutron setup. However, since the polarisation measurement of the deuteron is more delicate due to the small size of the polarisation signals, the modification of some basic components is needed. The reason for this is twofold: firstly the magnetic moment of the deuteron is smaller than that of the proton and, in addition, the interaction of the deuteron quadrupole moment with the electric field gradient in the sample broadens the deuteron polarisation signal. An accuracy $\delta P_p/P_p$ of 2 to 3% for the protons and $\delta P_D/P_D$ of 4 to 5% for the deuterons is expected in the polarisation measurement. It has also to be taken into account that the measured deuteron polarisation P_D is not equal to the neutron polarisation P_n. Assuming a 6 % admixture of the D-state of the deuteron, a calculation based on the Clebsch-Gordon coefficients leads to $P_n = 0.91\ P_D$. Several polarised proton and deuteron materials are available such as alcohols and deuterated alcohols (e.g. butanol C_4H_9OH), NH_3, ND_3 or ^{6}LiD. The most important criteria

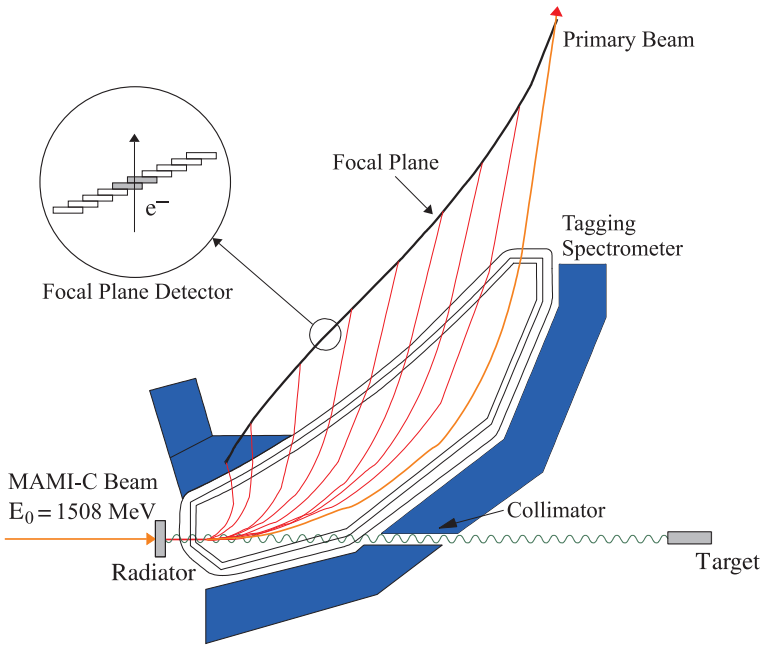

Figure 16: The Glasgow photon tagging spectrometer.

Figure 17: The new dilution refrigerator for the Crystal Ball Frozen Spin Target.

in the choice of material suitable for particle physics experiments are the degree of polarisation P and the ratio k of free polarisable nucleons to the total number of nucleons. Further requirements on polarised target materials are a short polarisation build-up time and a simple, reproducible target preparation. The polarisation resistance against radiation damage is not an issue for experiments with a low intensity tagged photon beam ($\dot{N}_\gamma \approx 5 \cdot 10^7\,\mathrm{s}^{-1}$) as will be used here. However, the limitations of a reduced relaxation time due to overheating of the target beads (Kapitza resistance) will have to be investigated.
Taking all properties together, butanol and deuterated butanol are the best material for this experiment. For protons we expect a maximum polarisation of $P_p = 90\%$ and an average polarisation of $P_p = 70\%$ in the frozen spin mode. Recently, a deuteron polarisation $P_D = 80\%$ was obtained with Trityl doped butanol targets at 2.5 T magnetic field in a ^{3}He/^{4}He dilution refrigerator. At a 0.4 T holding field an average neutron polarisation P_n (see above) of 50 % will be obtained. The filling factor for the ∼2 mm diameter butanol spheres into the 2 cm long, 2 cm diameter target container will be around 60%. The experience from the GDH runs in 1998 [5] shows that, with a total tagged photon flux of $5 \cdot 10^7$, relaxation times of about 200 hours can be expected. The polarisation has to be refreshed by microwave pumping every two days.
In conclusion, we estimate that we will achieve the following target parameters:

- Maximum total tagged photon flux in the energy range of 4.7% to 93.0% of E_0: $\dot{N}_\gamma \approx 5 \cdot 10^7\,\mathrm{s}^{-1}$, with relaxation time of 200 hours.
- Target proton density in 2 cm cell: $N_T \approx 9.1 \cdot 10^{22}\mathrm{cm}^{-2}$ (including dilution and filling factors)
- Average proton polarisation $P_p = 70\%$
- Target deuteron density in 2cm cell: $N_T \approx 9.4 \cdot 10^{22}\mathrm{cm}^{-2}$ (including dilution and filling factors)
- Average neutron polarisation $P_n = 50\%$

A.3 Crystal Ball Detector System

The central detector system consists of the Crystal Ball calorimeter combined with a barrel of scintillation counters for particle identification and two coaxial multiwire proportional counters for charged particle tracking. This central system provides position, energy and timing information for both charged and neutral particles in the region between 21° and 159° in the polar angle (θ) and over almost the full azimuthal (ϕ) range. At forward angles, less than 21°, reaction products are detected in the TAPS forward wall. The full, almost hermetic, detector system is shown schematically in Fig. 18 and the measured two-photon invariant mass spectrum is shown in Fig. 19.
The Crystal Ball detector (CB) is a highly segmented 672-element NaI(Tl), self triggering photon spectrometer constructed at SLAC in the 1970's. Each element is a truncated triangular pyramid, 41 cm (15.7 radiation lengths) long. The Crystal Ball has an energy resolution of $\Delta E/E = 0.020 \cdot E[GeV]^{0.36}$, angular resolutions of $\sigma_\theta = 2 \ldots 3°$ and $\sigma_\phi = \sigma_\theta / \sin\theta$ for electromagnetic showers [1]. The readout electronics for the Crystal Ball were completely renewed in 2003, and it now is fully equipped with SADCs which allow for the full sampling of pulse-shape element by element. In normal operation, the onboard summing capacity of these ADCs is used to enable dynamic pedestal subtraction and the provision of pedestal, signal and tail values for each element event-by-event. Each CB element is also newly equipped with multi-hit CATCH TDCs. The readout of the CB is effected in such a way as to allow for flexible triggering algorithms. There is an analogue sum of all ADCs, allowing for a total energy trigger, and also an OR of groups of

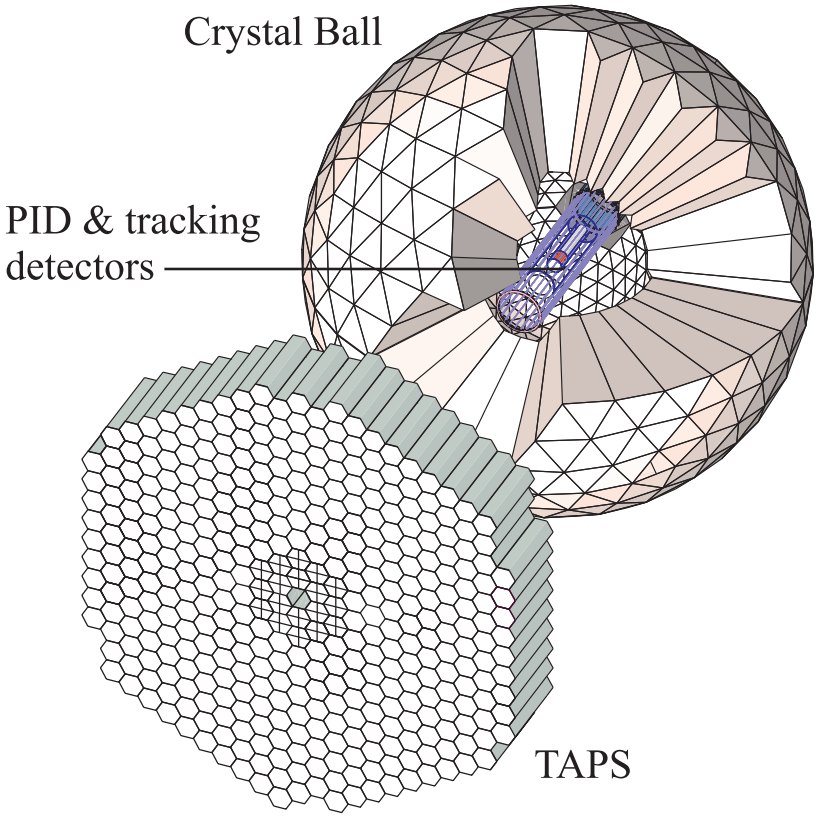

Figure 18: The A2 detector setup: The Crystal Ball calorimeter, with cut-away section showing the inner detectors, and the TAPS forward wall.

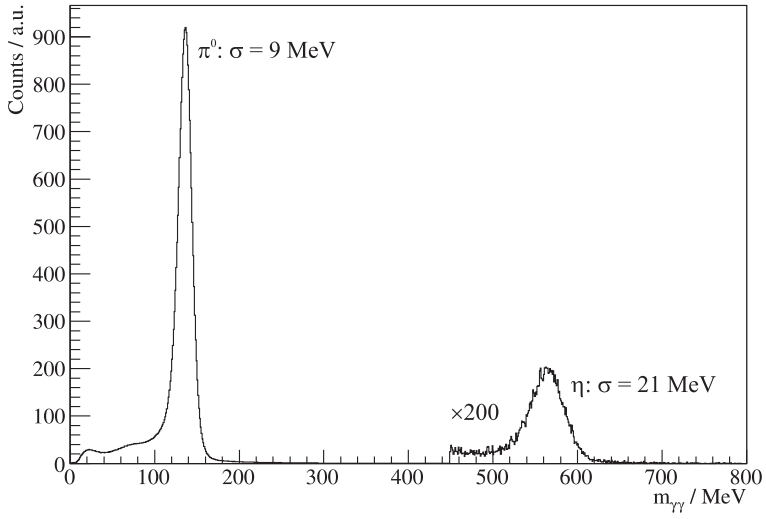

Figure 19: Two photon invariant mass spectrum for the CB/TAPS detector setup. Both η and π^0 mesons can be clearly seen.

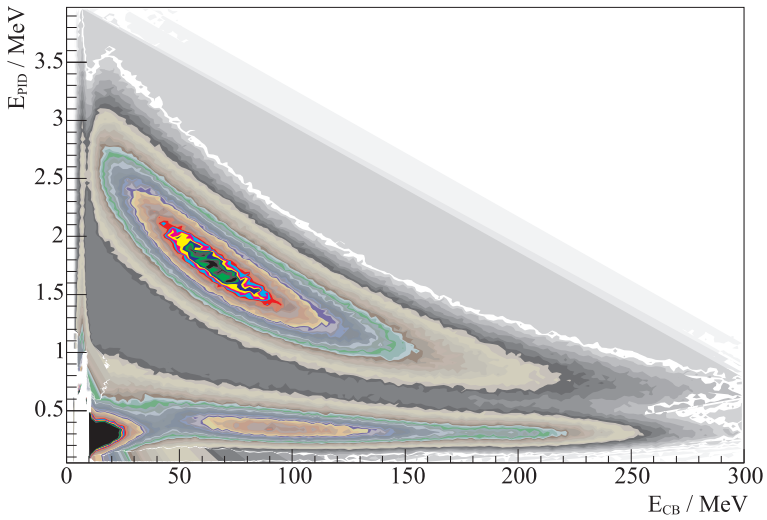

Figure 20: A typical $\Delta E/E$ plot from the Crystal Ball and the PID2 detector. The upper curved region is the proton locus, the lower region contains the pions and the peak towards the origin contains mostly electrons.

sixteen crystals to allow for a hit-multiplicity second-level trigger - ideal for use when searching for high multiplicity final states.

In order to distinguish between neutral and charged particles species detected by the Crystal Ball, the system is equipped with PID2, a barrel detector of twenty-four 50 mm long, 4 mm thick scintillators, arranged so that each PID2 scintillator subtends an angle of 15° in ϕ. By matching a hit in the PID2 with a corresponding hit in the CB, it is possible to use the locus of the $\Delta E, E$ combination to identify the particle species (Fig. 20). This is primarily used for the separation of charged pions, electrons and protons. The PID2 covers from 15° to 159° in θ.

The excellent CB position resolution for photons stems from the fact that a given photon triggers several crystals and the energy-weighted mean of their positions locates the photon position to better than the crystal pitch. For charged particles which deposit their energy over only one or two crystals, this is not so precise. Here the tracks of charged particles emitted within the angular and momentum acceptance of the CB detector will be reconstructed from the coordinates of point of intersections of the tracks with two coaxial cylindrical multiwire proportional chambers (MWPCs) with cathode strip readout. These MWPCs are similar to those installed inside the CB during the first round of MAMI-B runs [3]. The most significant difference is that all detector signals are taken at the upstream end of the MWPCs, minimising the material required and facilitating particle detection in the forward polar region.

A mixture of argon (79.5%), ethane (30%) and freon-CF_4 (0.5%) is used as the filling gas. This mixture is a compromise between charge multiplication and localization requirements imposed by the ionizing particle tracks.

Within each chamber both the azimuthal and the longitudinal coordinates of the avalanche will be evaluated from the centroid of the charge distribution induced on the cathode strips. The location of the hit wires(s) will be used to resolve ambiguities which arise from the fact that each pair of inner and outer strip cross each other twice. The expected angular resolution (rms) will be $\sim 2°$ in the polar emission angle θ and $\sim 3°$ in the azimuthal emission angle ϕ.

The MWPCs have been recently installed inside the CB frame and their calibration using both cosmic rays and test beam data is currently underway.

A.4 TAPS Forward Wall

The TAPS forward wall is composed of 384 BaF_2 elements, each 25 cm in length (12 radiation lengths) and hexagonal in cross section, with a diameter of 59 mm. The front of every TAPS element is covered by a 5 mm thick plastic veto scintillator. The single counter time resolution is $\sigma_t = 0.2$ ns, the energy resolution can be described by $\Delta E/E = 0.018 + 0.008/E[GeV]^{0.5}$ [1]. The angular resolution in the polar angle is better than 1°, and in the azimuthal angle it improves with increasing θ, being always better than $1/R$ radian, where R is the distance in centimeters from the central point of the TAPS wall surface to the point on the surface where the particle trajectory meets the detector. The TAPS readout was custom built for the beginning of the CB@MAMI program and is effected in such a way as to allow particle identification by Pulse Shape Analysis (PSA), Time Of Flight (TOF) and $\Delta E/E$ methods (using the energy deposit in the plastic scintillator to give ΔE). TAPS can also contribute to the CB multiplicity trigger and is currrently divided into upto six sectors for this purpose. The 2 inner rings of 18 BaF_2 elements have been replaced recently by 72 $PbWO_4$ crystals each 20 cm in length (22 radiation lengths). The higher granularity improves the rate capability as well as the angular resolution. The crystals are operated at room temperature. The energy resolution for photons is similar to BaF_2 under these conditions [6].

References

[1] S. Prakhov et al.: *Measurement of the Slope Parameter α for the $\eta \to 3\pi^0$ decay with the Crystal Ball dectector at the Mainz Microtron (MAMI-C)*, Phys. Rev. **C 79** (2009) 035204

[2] J.C. McGeorge et al.: *Upgrade of the Glasgow photon tagging spectrometer for Mainz MAMI-C*, Eur. Phys. J. **A 37** (2008) 129

[3] G. Audit et al.: *DAPHNE: a large-acceptance tracking detector for the study of photoreactions at intermediate energies*, Nucl. Instr. Meth. **A 301** (1991) 473

[4] A. Reiter et al.: *A microscope for the Glasgow photon tagging spectrometer in Mainz*, Eur. Phys. J. **A 30** (2006) 461

[5] A. Thomas et al.: *The GDH Experiment at MAMI*, Nucl. Phys. **B 79** (1999) 591

[6] R. Novotny et al.: *Scintillators for photon detection at medium energies - a comparative study of BaF_2, CeF_3 and $PbWO_4$*, Nucl. Instr. Meth. **A** 486 (2002) 131